The Astrophysical Journal Letters, 935:L18 (6pp), 2022 August 10 https://doi.org/10.3847/2041-8213/ac85ef

Near-infrared Accretion Signatures from the Circumbinary Planetary-mass Companion Delorme 1 (AB)b*

S. K. Betti[1,13], K. B. Follette[2], K. Ward-Duong[3], Y. Aoyama[4], G.-D. Marleau[5,6,7], J. Bary[8], C. Robinson[2], M. Janson[9], W. Balmer[10,11], G. Chauvin[12], and P. Palma-Bifani[12]
[1] Department of Astronomy, University of Massachusetts, Amherst, MA 01003, USA; sbetti@umass.edu
[2] Department of Physics and Astronomy, Amherst College, Amherst, MA 01003, USA
[3] Department of Astronomy, Smith College, Northampton, MA 01063, USA
[4] Kavli Institute for Astronomy and Astrophysics, Peking University, Beijing 100084, People's Republic of China
[5] Institut für Astronomie und Astrophysik, Universität Tübingen, Auf der Morgenstelle 10, D-72076 Tübingen, Germany
[6] Physikalisches Institut, Universität Bern, Gesellschaftsstr. 6, 3012 Bern, Switzerland
[7] Max-Planck-Institut für Astronomie, Königstuhl 17, D-69117 Heidelberg, Germany
[8] Department of Physics and Astronomy, Colgate University, Hamilton, NY 13346, USA
[9] Institutionen för astronomi, AlbaNova universitetscentrum, Stockholms universitet, SE-10691 Stockholm, Sweden
[10] The William H. Miller III Department of Physics & Astronomy, Johns Hopkins University, Baltimore, MD 21218, USA
[11] Space Telescope Science Institute, 3700 San Martin Drive, Baltimore MD 21218, USA
[12] Laboratoire Lagrange, Université Cote d'Azur, CNRS, Observatoire de la Cote d'Azur, F-06304 Nice, France
Received 2022 June 3; revised 2022 July 21; accepted 2022 August 2; published 2022 August 15

Abstract

Accretion signatures from bound brown dwarf and protoplanetary companions provide evidence for ongoing planet formation, and accreting substellar objects have enabled new avenues to study the astrophysical mechanisms controlling the formation and accretion processes. Delorme 1 (AB)b, a ∼30–45 Myr circumbinary planetary-mass companion, was recently discovered to exhibit strong Hα emission. This suggests ongoing accretion from a circumplanetary disk, somewhat surprising given canonical gas disk dispersal timescales of 5–10 Myr. Here, we present the first NIR detection of accretion from the companion in Paβ, Paγ, and Brγ emission lines from SOAR/TripleSpec 4.1, confirming and further informing its accreting nature. The companion shows strong line emission, with $L_{\rm line} \approx 1\text{–}6 \times 10^{-8}\,L_{\odot}$ across lines and epochs, while the binary host system shows no NIR hydrogen line emission ($L_{\rm line} < 0.32\text{–}11 \times 10^{-7}\,L_{\odot}$). Observed NIR hydrogen line ratios are more consistent with a planetary accretion shock than with local line excitation models commonly used to interpret stellar magnetospheric accretion. Using planetary accretion shock models, we derive mass accretion rate estimates of $\dot{M}_{\rm pla} \sim 3\text{–}4 \times 10^{-8}\,M_{\rm J}\ {\rm yr}^{-1}$, somewhat higher than expected under the standard star formation paradigm. Delorme 1 (AB)b's high accretion rate is perhaps more consistent with formation via disk fragmentation. Delorme 1 (AB)b is the first protoplanet candidate with clear (signal-to-noise ratio ∼5) NIR hydrogen line emission.

Unified Astronomy Thesaurus concepts: Planet formation (1241); Accretion (14); Stellar accretion disks (1579)

1. Introduction

The theory of magnetospheric accretion, whereby infalling inner disk material flows along stellar magnetic field lines and forms a shock in a young star's atmosphere, is well established and consistent with a range of observations (e.g., Koenigl 1991). X-ray emission originating from the shock front is absorbed and reradiated as excess optical/ultraviolet Balmer continuum (e.g., Valenti et al. 1993; Calvet & Gullbring 1998; Gullbring et al. 1998; Hartmann et al. 2016), while infalling gas exhibits line emission, including the Balmer, Paschen, and Brackett series hydrogen lines.

The same accretion process has been assumed to extend to substellar masses (e.g., Muzerolle et al. 2005; Alcalá et al. 2017), and accretion signatures from planetary-mass companions (PMCs) have been interpreted under the stellar paradigm. Recent discoveries of Hα accretion signatures in substellar companions—both brown dwarfs (BD) (e.g., SR12c; Santamaría-Miranda et al. 2018, 2019) and protoplanet candidates (e.g., PDS 70 b and c and LkCa 15 b; Sallum et al. 2015; Wagner et al. 2018; Haffert et al. 2019)—have provided incontrovertible evidence of accretion onto secondary objects in young systems. Combined with the first detections of circumplanetary disks (Benisty et al. 2021), these systems allow for the direct study of planet formation processes.

Recently, Eriksson et al. (2020) discovered strong hydrogen (Hα, Hβ) and helium emission lines suggestive of ongoing accretion from the PMC 2MASS J01033563–5515561(AB)b, also known as Delorme 1 (AB)b. Among the first imaged circumbinary PMCs, Delorme 1 (AB)b was discovered in the L' band by Delorme et al. (2013) at 1.″77 (84 au) separation, with an estimated mass of 12–14 $M_{\rm Jup}$, placing it at the deuterium-burning limit. Its host, Delorme 1 AB, is an M5.5 binary (separation of ∼0.″25 or 12 au; Delorme et al. 2013) at 47.2 ± 3 pc (Riedel et al. 2014) in the Tucana-Horologium association (Gagné et al. 2015), placing its age at ∼30–45 Myr.

* Based on observations obtained at the Southern Astrophysical Research (SOAR) telescope, which is a joint project of the Ministério da Ciência, Tecnologia e Inovações (MCTI/LNA) do Brasil, the US National Science Foundation's NOIRLab, the University of North Carolina at Chapel Hill (UNC), and Michigan State University (MSU).
[13] Visiting astronomer, Cerro Tololo Inter-American Observatory at NSF's NOIRLab, which is managed by the Association of Universities for Research in Astronomy (AURA) under a cooperative agreement with the National Science Foundation.

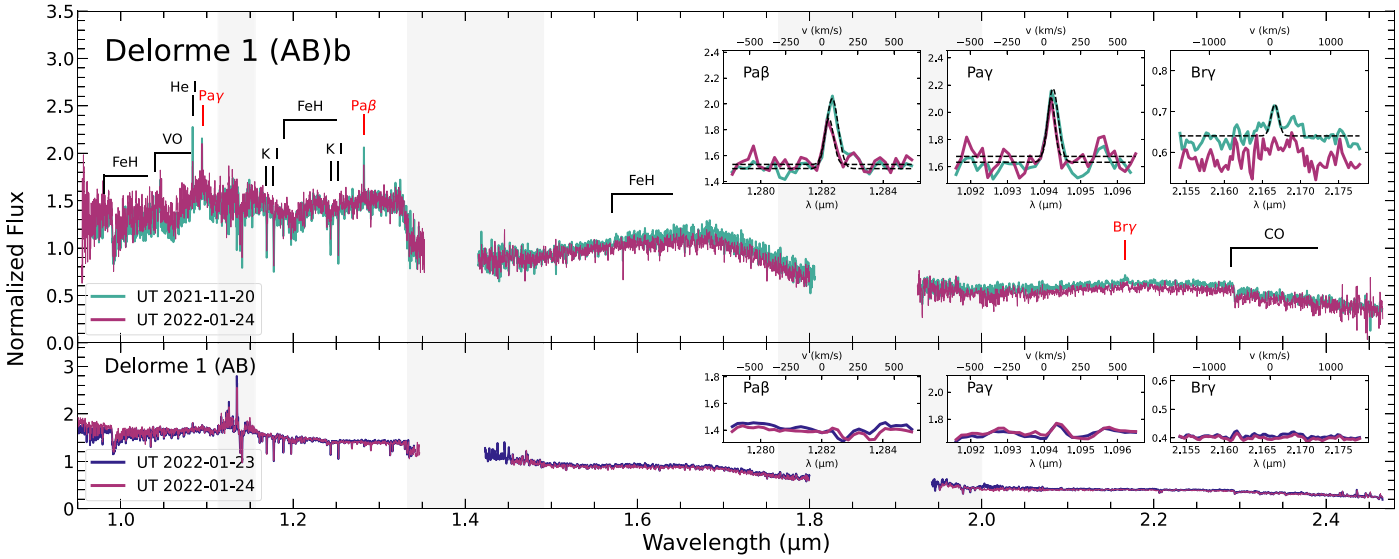

Figure 1. TripleSpec 4.1 *JHK*-band spectra of Delorme 1 (AB)b (top; green: UT 2021-11-20, magenta: UT 2022-01-24) and Delorme 1 AB (bottom; blue: UT 2022-01-23, magenta: UT 2022-01-24) The NIR emission lines, Paγ, Paβ, and Brγ, are highlighted with red labels. The lines are shown in greater detail in the inset images for the companion (top; with best-fit Gaussians shown by dashed black lines) and binary host (bottom). Other atomic and molecular features are labeled in black. Gray bands indicate regions of high atmospheric absorption.

While the system shows evidence of youth, including an overluminous central binary (Riedel et al. 2014), red JHK_s colors (similar to other young bound nonaccreting companions; Riedel et al. 2014), and low surface gravity (Liu et al. 2016), ongoing PMC accretion at 30–45 Myr is possible, as lower-mass objects have been found to have long disk dispersal timescales (Luhman 2022).[14]

In this Letter, we present the first detection of near-infrared (NIR) emission lines from Delorme 1 (AB)b, corroborating the claim of ongoing companion accretion and confirming the lack of accretion in the host binary system. This is the first accreting PMC with Paβ, Paγ, and Brγ detections and provides a critical benchmark for future NIR accretion studies of PMCs. NIR line ratios provide an important probe of the physical properties of the emitting region that can inform accretion paradigms.

2. Observations and Reductions

Delorme 1 (AB)b was observed with the TripleSpec 4.1 Near-IR spectrograph (Schlawin et al. 2014) on the Southern Astrophysical Research (SOAR) Telescope during two observing runs in 2021–2022 (ID: 2021B–0311). TripleSpec 4.1 covers 0.8–2.47 μm at moderate resolution (R∼3500) with a fixed $1\farcs1 \times 28''$ slit. Both observations were taken in good weather conditions, with seeing around $0\farcs95$–$1\farcs0$, with the slit aligned to the parallactic angle. Delorme 1 (AB)b was observed on 2021 November 20 (epoch 1) at an airmass of 1.2. Sixteen 180 s exposures were taken in an ABBA cycle, for a total exposure time of 2880 s, yielding a final reduced spectrum with a mean signal-to-noise ratio (S/N) of ∼90 at H-band. On 2022 January 24 (epoch 2), we observed Delorme 1 (AB)b at an airmass of 1.27 with an identical observational strategy and total integration time, with the reduced spectrum achieving a mean S/N of ∼60 at the H band. We observed the binary Delorme 1 AB on 2022 January 23 (airmass 1.34) and on 2022 January 24 (airmass 1.65). We took eight 30 s exposures in an ABBA cycle, for a total of 240 s each night, yielding average final spectrum S/Ns of 270 and 300 at the H band. As the seeing on January 23 was $\sim 1\farcs3$, we were not able to sufficiently resolve the companion and did not attempt to observe it.

Spectra were reduced using a TripleSpec 4.1 version of SpeXtool (Cushing et al. 2004) following the standard procedure: subtraction of A and B frames for sky removal, order identification, spectral extraction, and wavelength calibration from arc lamps. The orders were merged and areas of significant atmospheric absorption removed. A spectrophotometric standard (HIP 6364, A0V) was observed before and after Delorme 1 for both telluric correction and flux calibration, following Vacca et al. (2003) using the SpeXtool `xtellcor` software. Due to its close distance (47.2 ± 3.1 pc; Riedel et al. 2014), Delorme 1 resides in the Local Bubble (area of low interstellar extinction; Sfeir et al. 1999); therefore, we assume zero reddening.

3. Results

We detect strong Paβ, Paγ, and Brγ emission lines (Figure 1) in Delorme 1 (AB)b in both epochs. Hydrogen emission lines are not detected in the host binary (see Table 1 for line flux upper limits), providing strong confirmation they are unique to the companion.

We compute equivalent widths (EW), fluxes ($F_{\rm line}$), and luminosities ($L_{\rm line}$) for each line and epoch (Table 1). Line fluxes are computed by integrating under a best-fit Gaussian profile after subtracting a linear fit to the local continuum. The uncertainty on the line is a function of the scatter in the continuum and the best-fit Gaussian given by

$$\sigma = \sqrt{N_{\rm pix}} \times F_{\rm noise} \times \Delta\lambda, \quad (1)$$

where $N_{\rm pix}$ is the number of pixels within 3× FWHM, $F_{\rm noise}$ is the rms of the local continuum, and $\Delta\lambda$ is the wavelength resolution per pixel at each line. EWs are obtained from the

[14] Luhman (2022) found that in the 15–21 Myr Lower Centaurus Crux and Upper Centaurus Lupus association, disk fractions increase with decreasing mass, from 0.7% to 9%, indicating lower-mass stars can retain disks far longer than originally estimated (∼10 Myr).

Table 1
Delorme 1 (AB)b Line Characteristics

Line	EW (Å)	$F_{\rm line}$ (10^{-16} erg s cm^{-2})	$L_{\rm line}$ ($10^{-8} L_\odot$)	Stellar Scaling[a]		Planetary Scaling[b]		Delorme 1 AB $F_{\rm line}$ (10^{-15} erg s cm^{-2})
				$\log(L_{\rm acc})$ ($L_\odot$)	$\log(\dot{M})$ ($M_{\rm J}$ yr^{-1})	$\log(L_{\rm acc})$ ($L_\odot$)	$\log(\dot{M})$ ($M_{\rm J}$ yr^{-1})	
UT 2021-11-20								
Paγ	-1.95 ± 0.74	6.82 ± 1.33	4.75 ± 1.11	-5.50 ± 0.53	-8.82 ± 0.53	-3.94 ± 0.30	-7.27 ± 0.30	<3.67
Paβ	-2.31 ± 0.88	8.05 ± 1.49	5.60 ± 1.27	-4.92 ± 0.62	-8.25 ± 0.62	-4.02 ± 0.30	-7.35 ± 0.30	<3.71
Brγ	-2.08 ± 1.11	1.64 ± 0.56	1.14 ± 0.42	-5.43 ± 0.94	-8.75 ± 0.96	-3.91 ± 0.30	-7.24 ± 0.30	<1.01
UT 2022-01-24								
Paγ	-1.24 ± 0.47	2.94 ± 0.77	2.05 ± 0.61	-5.95 ± 0.55	-9.28 ± 0.56	-4.25 ± 0.30	-7.58 ± 0.30	<7.91
Paβ	-1.44 ± 0.62	3.49 ± 0.85	2.43 ± 0.67	-5.31 ± 0.64	-8.64 ± 0.65	-4.33 ± 0.30	-7.67 ± 0.30	<6.56
Brγ	···	<0.74	<0.52	<−5.81	<−9.17	<−4.20	<−7.53	<1.86

Notes.
[a] $L_{\rm acc}$–$L_{\rm line}$ scaling relation from Alcalá et al. (2017).
[b] $L_{\rm acc}$–$L_{\rm line}$ scaling relation from Aoyama et al. (2021).

ratio of line fluxes to the average local continuum level within a 50 Å window on either side of the line. We estimate EW uncertainties following Vollmann & Eversberg (2006).

We do not detect Brγ in epoch 2, potentially due to poorer seeing conditions. For nondetected lines, we calculate $F_{\rm line}$ upper limits as $F_{\rm line}^{\rm upp} = 3\sigma$.

During magnetospheric accretion, the infalling column of gas is heated to $\sim 10^4$ K, producing broad emission lines (Hartmann et al. 2016) such as Paβ, Paγ, and Brγ. The gas travels at freefall velocity and heats to 10^6 K when it shocks at the stellar photosphere, fully ionizing and preventing the formation of hydrogen line emission. In contrast, recent simulations of accreting PMCs (Aoyama et al. 2018, 2020) suggest differences in the physical conditions of the shocked region. Due to smaller masses and lower surface gravities, accreting gas travels at lower freefall velocities, leading to a non-fully ionized postshock region. This results in shock-heated accreting gas capable of hydrogen line emission (Aoyama et al. 2018). In other words, the detections of Paschen and Brackett series emission from accreting objects are an unambiguous sign of accretion; however, the dominant source of line emission may be either the infalling accretion column or the postshock region. Given this ambiguity, we estimate accretion rates for Delorme 1 (AB)b following both families of accretion models, and discuss the differences below. The mass accretion rate is given by

$$\dot{M} = \left(1 - \frac{R_\star}{R_{\rm in}}\right)^{-1} \frac{L_{\rm acc} R_\star}{G M_\star}, \quad (2)$$

where $R_{\rm in}$ is the inner disk radius, assumed to be 5 $R_\star$ (e.g., Gullbring et al. 1998; Herczeg & Hillenbrand 2008; Rigliaco et al. 2012; Alcalá et al. 2017), $R_\star$ is the radius of the accreting object, $M_\star$ is its mass, and $L_{\rm acc}$ is the estimated accretion luminosity.

Total accretion luminosity has been found to strongly correlate with emission line luminosities in T Tauri stars (Rigliaco et al. 2012; Alcalá et al. 2014, 2017) as

$$\log(L_{\rm acc}/L_\odot) = a \times \log(L_{\rm line}/L_\odot) + b, \quad (3)$$

where a and b are the fit coefficients for each line. These relationship can be used to estimate $\dot{M}$ from a single accretion-tracing line. However, Aoyama et al. (2020, 2021) argue that the $L_{\rm line}$–$L_{\rm acc}$ relationships are not valid for planetary-mass objects because of the different physical conditions of the emitting region. Aoyama et al. (2021) derived new theoretical $L_{\rm acc}$–$L_{\rm line}$ relationships expected for PMCs based on the Aoyama et al. (2018) shock models. We refer to all accretion luminosities and mass accretion rates derived from the Alcalá et al. (2017) $L_{\rm acc}$–$L_{\rm line}$ scaling relations as "stellar" (e.g., $L_{\rm acc,\,ste}/\dot{M}_{\rm ste}$) and those derived from Aoyama et al. (2021) as "planetary" (e.g., $L_{\rm acc,\,pla}/\dot{M}_{\rm pla}$) for ease in distinguishing between the two.

Following Eriksson et al. (2020), we assume a companion mass of $M_p = 0.012\,M_\odot$ and radius $R_p = 0.163\,R_\odot$. We calculate $L_{\rm acc}$ following the $L_{\rm acc}$–$L_{\rm line}$ scaling relations calibrated empirically for stars (Paβ: $(a, b) = (1.06, 2.76)$, Paγ: $(a, b) = (1.24, 3.58)$, Brγ: $(a, b) = (1.19, 4.02)$) by Alcalá et al. (2017) and theoretically for PMCs (Paβ: $(a, b) = (0.86, 2.21)$, Paγ: $(a, b) = (0.85, 2.28)$, Brγ: $(a, b) = (0.85, 2.84)$) by Aoyama et al. (2021). This allows us to directly compare our NIR-derived results to the accretion rates estimated by Eriksson et al. (2020).

Our $\dot{M}$ estimates are given in Table 1 for both the "stellar" and "planetary" relations. $\dot{M}$ estimates are relatively consistent among lines and epochs under each scaling relation; however, the Aoyama et al. (2021) models predict $\dot{M}$'s that are systematically higher by several orders of magnitude.

On average, using the stellar scaling relations of Alcalá et al. (2017), we find a $\log(\dot{M}_{\rm ste})$ of $-8.53 \pm 0.28\,M_{\rm J}\,{\rm yr}^{-1}$ for epoch 1 and $-8.85 \pm 0.28\,M_{\rm J}\,{\rm yr}^{-1}$ for epoch 2. Using the Aoyama et al. (2021) planetary-shock-model relations, we find $\log(\dot{M}_{\rm pla}) = -7.38 \pm 0.23\,M_{\rm J}\,{\rm yr}^{-1}$ and $-7.19 \pm 0.31\,M_{\rm J}\,{\rm yr}^{-1}$ for epochs 1 and 2, respectively.

4. Discussion

We have presented mass accretion rate estimates for Delorme 1 (AB)b derived from NIR hydrogen emission lines under two assumed scalings of $L_{\rm line}$ to $L_{\rm acc}/\dot{M}$. Accretion rate estimates for individual NIR lines agree with one another within the "planetary" and "stellar" accretion paradigms, with the exception of the "stellar" Paβ accretion rate, which is

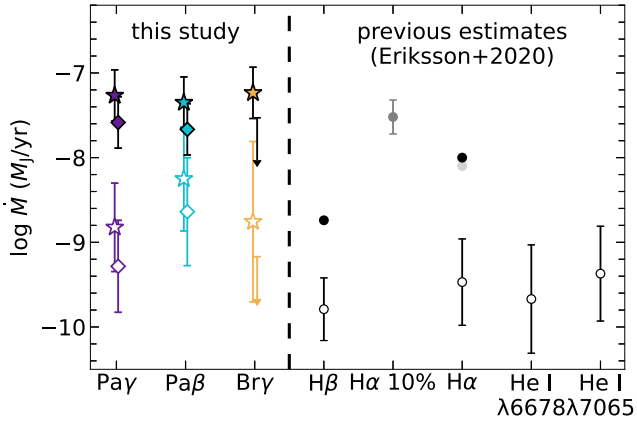

Figure 2. Accretion rates for individual emission lines. Circles indicate data from Eriksson et al. (2020). Stars and diamonds represent our epochs 1 and 2, respectively. Accretion rates derived using both "stellar" empirical scaling relations (open symbols; Alcalá et al. 2017) and "planetary" accretion models (filled symbols; Aoyama et al. 2021) are shown. $\dot{M}$(Hα) is also estimated using the line luminosity model of Thanathibodee et al. (2019, light gray). $\dot{M}$ (Hα 10%) is estimated using a "stellar" empirical relation (dark gray; Natta et al. 2004).

marginally inconsistent with the other "stellar" accretion estimates.

In Figure 2, we compare our NIR observations (diamonds/stars) with the marginally resolved Hα observations of Eriksson et al. (2020) (gray/black circles) and convert each to $\dot{M}$ using both "stellar" (unfilled symbols; Alcalá et al. 2017; dark gray, Natta et al. 2004) and "planetary" (filled symbols; Aoyama & Ikoma 2019; light gray, Thanathibodee et al. 2019) scaling relations. Hα can originate from chromospheric activity, complicating its interpretation. Eriksson et al. (2020) found that the contribution to the Hα line profile due to chromospheric activity should be minimal at this age, pointing toward Delorme 1 (AB)b experiencing ongoing accretion. We find that our NIR $\dot{M}$'s generally agree with the Eriksson et al. (2020) estimates within uncertainties, albeit with slightly higher $\dot{M}$ values relative to the Balmer series, though our Paβ measurement is marginally inconsistent at the 1σ level. Given the strength of the companion's NIR EWs relative to diagnostics measured for active low-mass stars ($\sim$0.04–0.05 Å; e.g., Schöfer et al. 2019), our results are most consistent with the presence of PMC accretion.

We find agreement between $\dot{M}_{\rm pla}$ and $\dot{M}$(Hα 10%); both are $\sim$1.5 mag higher than $\dot{M}_{\rm ste}$. As $\dot{M}$(Hα 10%) does not rely on scaling relationships, accurate continuum subtraction, or extinction, it is considered a robust independent measure of accretion (White & Basri 2003; Stelzer et al. 2007), including for the lowest-mass accreting protoplanets (e.g., PDS 70 b; Haffert et al. 2019). As noted by Alcalá et al. (2014), the empirical relationship between the Hα 10% width and $\dot{M}$ (Natta et al. 2004) has considerable scatter, and line luminosities should also be used when possible. However, the strong agreement between $\dot{M}$(Hα 10%) and $\dot{M}_{\rm pla}$ could indicate that $\dot{M}_{\rm pla}$ is a more accurate estimate of $\dot{M}$ for Delorme 1 (AB)b. The marginal inconsistency in $\dot{M}_{\rm ste}$ could be a result of applying stellar scaling relations to an object accreting under a different paradigm; this is not seen in the $\dot{M}_{\rm pla}$'s.

To independently determine the accretion paradigm most consistent with Delorme 1 (AB)b without a reliance on scaling relations, line ratios can be used. NIR hydrogen lines are ideal for measuring accretion line ratios (see Bary et al. 2008; Edwards et al. 2013) due to their small line opacities, resulting in little blue- or redshifted absorption from winds or infalling gas (Folha & Emerson 2001; Edwards et al. 2006). By comparing observed line ratios to accretion model prediction, we can probe physical conditions of the emitting region such as number density, temperature, and infall velocity. Line ratios have discriminating power between different physical line emission sources, as different accretion models predict different line ratios. To this end, we consider two models: the local line excitation model of Kwan & Fischer (2011) and the planetary-shock model of Aoyama et al. (2018). As shown in Figure 3, the predicted line ratios of postshock gas in a planetary atmosphere (planetary paradigm; Aoyama et al. 2018, purple/yellow circles) can vary from those predicted by local line excitation models developed to describe infalling accretion columns of T Tauri stars (stellar paradigm; Kwan & Fischer 2011, green/blue squares), allowing us to infer which model better matches observations, though there is some overlap for lower densities, where we are not able to distinguish between accretion paradigms. We calculate line ratios for each line pair and epoch (star/diamond symbols) over the whole emission range.[15] In panel (d), we include ratios with respect to published Hα emission for context, noting these observations were not obtained contemporaneously with our NIR data. Line ratios may be affected by intrinsic and instrumental variability; therefore, the inconsistency of the Hα ratio with either model grid may not be indicative of variability in the physical conditions of the emitting region.

For all measurements, observed line ratios fall nearest the Aoyama et al. (2018) models and consistently diverge from the Kwan & Fischer (2011) models, suggesting that planetary scaling relations are likely more appropriate in this situation. Therefore, we use the Aoyama et al. (2021) models and relations for further analysis.

We extract all model physical input parameters consistent with observed line ratios within uncertainties. We find that the best-fitting models have preshock velocities of 70–170 km s^{-1} and number densities of 10^{13}–10^{14} cm^{-3}. While the preshock velocity is consistent with measured $\dot{M}$'s and assumed mass (and radius; see Figure 13 of Aoyama et al. 2020), the number density is higher than expected for the measured $\dot{M}$ assuming a pure planetary-shock model. This could be explained by shock emission with a low filling factor resulting from a magnetospheric accretion flow, absorption in the postshock region (Hashimoto et al. 2020), strong accretion column extinction (Marleau et al. 2022, though they found that the $\dot{M}$ is too low for absorption by either gas or dust in the accretion flow), or circumplanetary disk extinction in the line of sight (Aoyama et al. 2020). High-resolution ($R \sim$ 10,000) spectra will help disentangle the accretion flow geometry and shed light on the nature of the accretion shock, as resolved line profiles can distinguish between geometries (Aoyama et al. 2020; Marleau et al. 2022).

In Figure 4, we show the $\dot{M}$–M relation for all known accreting substellar objects, together with low-mass stars (S. K. Betti et al., in preparation). The $\dot{M}_{\rm pla}$'s for Delorme 1 (AB)b lie above the canonical $\dot{M} \sim M^{2.1}$ (Muzerolle et al. 2005) T Tauri star relation consistent with formation via collapsing prestellar cores. The mass accretion rates are similar to other bound

[15] In T Tauri stars, winds and outflow absorption can affect line ratios. As such, residual line profiles selected over regions with no opacity effects are used to calculate line ratios (see Edwards et al. 2013). However, these are assumed to be negligible in PMCs.

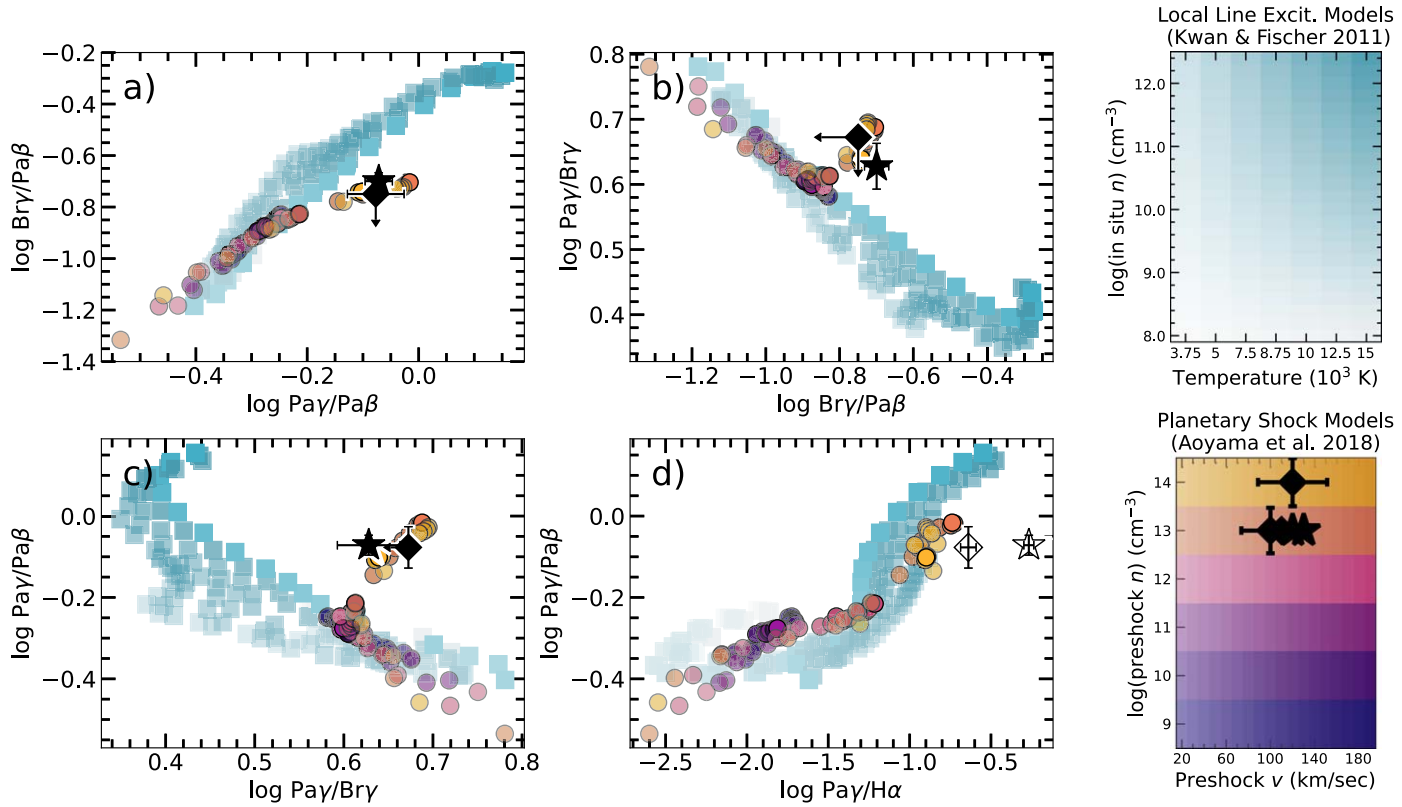

Figure 3. Predicted line ratios for local line excitation ("stellar"; Kwan & Fischer 2011, blue squares), and accretion shock emission ("planetary"; Aoyama et al. 2018, purple/yellow circles) models. Delorme 1 (AB)b's NIR line ratios (panels (a)–(c)) are shown in black with markers (stars, diamonds) indicating epoch as in Figure 2. Panel (d) shows Paγ/Hα line ratios, with Delorme 1 (AB)b values (unfilled markers) derived from our Paγ observations and the noncontemporaneous Hα measurement of Eriksson et al. (2020).

PMCs (black squares), whose previous accretion rate estimations mostly come from Hα line luminosity or the Hα 10% width. The location of these bound PMCs in $\dot{M}$–M space is consistent with model predictions of PMC formation through disk fragmentation in disks with low viscosities (Stamatellos & Herczeg 2015). These models predict higher accretion rates; companions that form in dynamically unstable systems have larger than expected gas mass reservoirs, allowing them to accrete more material (Stamatellos & Herczeg 2015) for longer. The high $\dot{M}$ observed for Delorme 1 (AB)b suggests that it may have formed via disk fragmentation. Its $\dot{M}$ is most consistent with Stamatellos & Herczeg (2015) models with low disk viscosity ($\alpha \sim 0.001$) and is comparable to PMCs with similar masses such as GSC 06214–00210 b, GQ Lup b, and DH Tau b, all of which have been theorized to have formed via disk fragmentation (Zhou et al. 2014; Stamatellos & Herczeg 2015).

In summary, the strong Paβ, Paγ, and Brγ emission seen from Delorme 1 (AB)b indicates strong ongoing mass accretion onto the PMC. Utilizing line ratios, we find that the NIR hydrogen emission is most consistent with models of planetary-shock accretion, though the high predicted number density does not exclude magnetospheric accretion from occurring as well on the planetary surface. We conclude that higher $\dot{M}$ estimates derived from planetary scaling relations are more likely to reflect the true accretion rate, and the position of Delorme 1 (AB)b in $\dot{M}$–M space is consistent with formation via disk fragmentation. This would account for its high accretion rate, which is consistent with low disk viscosity, likely resulting in slower disk evolution and perhaps explaining why this 30–45 Myr object is still actively accreting (potentially a "Peter Pan disk"; Silverberg et al. 2020). Detailed modeling of the planetary surface and disk will provide a clearer understanding of Delorme 1 (AB)b, and future observations of a wider range of line ratios will help constrain the nature of the accretion shock. Forthcoming work (S. K. Betti et al. 2022, in preparation) will present detections of NIR accretion for a comprehensive sample of accreting BDs and PMCs as well as observational $L_{\rm acc}$–$L_{\rm line}$ empirical relationships for the substellar regime in order to help constrain substellar formation mechanisms. Delorme 1 (AB)b is a benchmark accreting PMC, with current observations and theoretical models suggesting the nature of its emission is in the planetary regime.

We thank the anonymous referee for their careful review. We thank the SOAR support scientist, CTIO scientist Sean Points, for allocating some engineering time for our observations. S.K. B. and K.B.F. acknowledge support from NSF AST-2009816. G.D.M. acknowledges the support of the DFG priority program SPP 1992 "Exploring the Diversity of Extrasolar Planets" (MA 9185/1) and from the Swiss National Science Foundation under grant 200021_204847 "PlanetsInTime." Parts of this work have been carried out within the framework of the NCCR PlanetS supported by the Swiss National Science Foundation.

Facilities: SOAR (TripleSpec 4.1).

Software: astropy (Astropy Collaboration et al. 2013; Astropy Collaborationn et al. 2018), specutils (Earl et al. 2022), Spextool (Vacca et al. 2003; Cushing et al. 2004), Matplotlib (Hunter 2007).

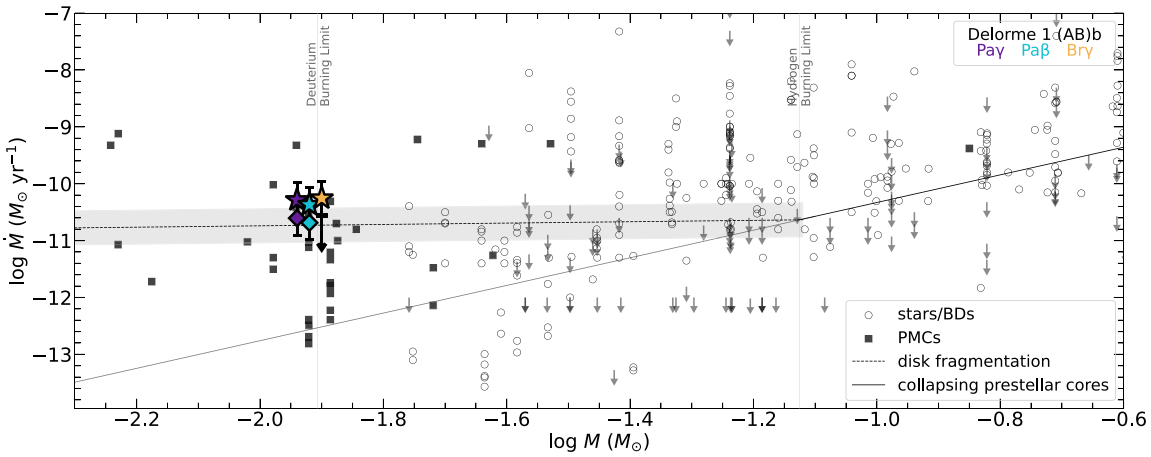

Figure 4. Mass accretion rate vs. mass for all known isolated substellar accretors (gray), PMCs (black squares), and a representative sample of low-mass stars. Delorme 1 (AB)b's NIR-derived $\dot{M}$ is highlighted (colored markers, symbol as in Figure 2). The canonical $\dot{M} \propto M^{2.1}$ (Muzerolle et al. 2005) relation for higher-mass objects (consistent with formation via collapsing prestellar cores) is shown (solid line) and a predicted relation for substellar objects formed via disk fragmentation (dashed line, $\alpha \sim 0.001$, Stamatellos & Herczeg 2015). Delorme 1 AB(b) Paγ and Brγ measurements have been offset in mass for clarity.

ORCID iDs

S. K. Betti https://orcid.org/0000-0002-8667-6428
K. B. Follette https://orcid.org/0000-0002-7821-0695
K. Ward-Duong https://orcid.org/0000-0002-4479-8291
Y. Aoyama https://orcid.org/0000-0003-0568-9225
G.-D. Marleau https://orcid.org/0000-0002-2919-7500
J. Bary https://orcid.org/0000-0001-8642-5867
C. Robinson https://orcid.org/0000-0003-1639-510X
M. Janson https://orcid.org/0000-0001-8345-593X
W. Balmer https://orcid.org/0000-0001-6396-8439
G. Chauvin https://orcid.org/0000-0003-4022-8598
P. Palma-Bifani https://orcid.org/0000-0002-6217-6867

References

Alcalá, J. M., Natta, A., Manara, C. F., et al. 2014, A&A, 561, A2
Alcalá, J. M., Manara, C. F., Natta, A., et al. 2017, A&A, 600, A20
Aoyama, Y., & Ikoma, M. 2019, ApJL, 885, L29
Aoyama, Y., Ikoma, M., & Tanigawa, T. 2018, ApJ, 866, 84
Aoyama, Y., Marleau, G.-D., Ikoma, M., & Mordasini, C. 2021, ApJL, 917, L30
Aoyama, Y., Marleau, G.-D., Mordasini, C., & Ikoma, M. 2020, arXiv:2011.06608
Astropy Collaboration, Robitaille, T. P., Tollerud, E. J., et al. 2013, A&A, 558, A33
Astropy Collaboration, Price-Whelan, A. M., Sipőcz, B. M., et al. 2018, AJ, 156, 123
Bary, J. S., Matt, S. P., Skrutskie, M. F., et al. 2008, ApJ, 687, 376
Benisty, M., Bae, J., Facchini, S., et al. 2021, ApJL, 916, L2
Calvet, N., & Gullbring, E. 1998, ApJ, 509, 802
Cushing, M. C., Vacca, W. D., & Rayner, J. T. 2004, PASP, 116, 362
Delorme, P., Gagné, J., Girard, J. H., et al. 2013, A&A, 553, L5
Earl, N., Tollerud, E., Jones, C., et al. 2022, astropy/specutils: V1.7.0, v1.7.0,, Zenodo, doi:10.5281/zenodo.6207491
Edwards, S., Fischer, W., Hillenbrand, L., & Kwan, J. 2006, ApJ, 646, 319
Edwards, S., Kwan, J., Fischer, W., et al. 2013, ApJ, 778, 148
Eriksson, S. C., Asensio Torres, R., Janson, M., et al. 2020, A&A, 638, L6
Folha, D. F. M., & Emerson, J. P. 2001, A&A, 365, 90
Gagné, J., Lafrenière, D., Doyon, R., Malo, L., & Artigau, É. 2015, ApJ, 798, 73
Gullbring, E., Hartmann, L., Briceño, C., & Calvet, N. 1998, ApJ, 492, 323
Haffert, S. Y., Bohn, A. J., de Boer, J., et al. 2019, NatAs, 3, 749
Hartmann, L., Herczeg, G., & Calvet, N. 2016, ARA&A, 54, 135
Hashimoto, J., Aoyama, Y., Konishi, M., et al. 2020, AJ, 159, 222
Herczeg, G. J., & Hillenbrand, L. A. 2008, ApJ, 681, 594
Hunter, J. D. 2007, CSE, 9, 90
Koenigl, A. 1991, ApJL, 370, L39
Kwan, J., & Fischer, W. 2011, MNRAS, 411, 2383
Liu, M. C., Dupuy, T. J., & Allers, K. N. 2016, ApJ, 833, 96
Luhman, K. L. 2022, AJ, 163, 25
Marleau, G. D., Aoyama, Y., Kuiper, R., et al. 2022, A&A, 657, A38
Muzerolle, J., Luhman, K. L., Briceño, C., Hartmann, L., & Calvet, N. 2005, ApJ, 625, 906
Natta, A., Testi, L., Muzerolle, J., et al. 2004, A&A, 424, 603
Riedel, A. R., Finch, C. T., Henry, T. J., et al. 2014, AJ, 147, 85
Rigliaco, E., Natta, A., Testi, L., et al. 2012, A&A, 548, A56
Sallum, S., Follette, K. B., Eisner, J. A., et al. 2015, Natur, 527, 342
Santamaría-Miranda, A., Cáceres, C., Schreiber, M. R., et al. 2018, MNRAS, 475, 2994
Santamaría-Miranda, A., Cáceres, C., Schreiber, M. R., et al. 2019, MNRAS, 488, 5852
Schlawin, E., Herter, T. L., Henderson, C., et al. 2014, Proc. SPIE, 9147, 91472H
Schöfer, P., Jeffers, S. V., Reiners, A., et al. 2019, A&A, 623, A44
Sfeir, D. M., Lallement, R., Crifo, F., & Welsh, B. Y. 1999, A&A, 346, 785
Silverberg, S. M., Wisniewski, J. P., Kuchner, M. J., et al. 2020, ApJ, 890, 106
Stamatellos, D., & Herczeg, G. J. 2015, MNRAS, 449, 3432
Stelzer, B., Scholz, A., & Jayawardhana, R. 2007, ApJ, 671, 842
Thanathibodee, T., Calvet, N., Bae, J., Muzerolle, J., & Hernández, R. F. 2019, ApJ, 885, 94
Vacca, W. D., Cushing, M. C., & Rayner, J. T. 2003, PASP, 115, 389
Valenti, J. A., Basri, G., & Johns, C. M. 1993, AJ, 106, 2024
Vollmann, K., & Eversberg, T. 2006, AN, 327, 862
Wagner, K., Follete, K. B., Close, L. M., et al. 2018, ApJL, 863, L8
White, R. J., & Basri, G. 2003, ApJ, 582, 1109
Zhou, Y., Herczeg, G. J., Kraus, A. L., Metchev, S., & Cruz, K. L. 2014, ApJL, 783, L17